Journal of Power Sources 244 (2013) 354–362

Contents lists available at SciVerse ScienceDirect

Journal of Power Sources

journal homepage: www.elsevier.com/locate/jpowsour

Development of all-solid-state lithium battery using quasi-solidified tetraglyme–lithium bis(trifluoromethanesulfonyl)amide–fumed silica nano-composites as electrolytes

Atsushi Unemoto*, Takahiro Matsuo, Hideyuki Ogawa, Yoshiyuki Gambe, Itaru Honma

Institute of Multidisciplinary Research for Advanced Materials, Tohoku University, 2-1-1 Katahira, Aoba-ku, Sendai 980-8577, Japan

HIGHLIGHTS

- Quasi-solid-state electrolyte containing G4/LiTFSA are prepared.
- Quasi-solid-state electrolyte has solid-like appearances.
- Quasi-solid-state electrolyte has liquid-like conductivity and diffusivity.
- All-solid-state cell exhibited noticeable charge–discharge performance.
- Concentration polarization resistance limited the power density.

ARTICLE INFO

Article history:
Received 24 October 2012
Received in revised form
30 December 2012
Accepted 1 January 2013
Available online 21 January 2013

Keywords:
Quasi-solid-state electrolyte
All-solid-state lithium battery
Glyme–Li-salt equimolar complex
Transport
Anodic stability

ABSTRACT

A quasi-solid-state electrolyte consisting of tetraethylene glycol dimethyl ether (tetraglyme, G_4)/lithium bis(trifluoromethanesulfonyl)amide (LiTFSA) mixtures together with fumed silica nanoparticles was prepared for use as the electrolyte of an all-solid-state lithium rechargeable battery. Via the liquid route, we have succeeded in fabricating a quasi-solid-state electrolyte regardless of the high concentration of G_4/Li-TFSA such as 75 vol%. It was found that the conductivities, the self-diffusion coefficients and the structure of the G_4/Li-TFSA complex in the quasi-solid-state composite are essentially similar to those of the bulks regardless of the solid-like appearance. Compared to the quasi-solid-state electrolytes containing the conventional room temperature ionic liquids (RTILs), the ones containing the equimolar G_4/LiTFSA complex exhibited a higher stability to the lithium electrodes. The all-solid-state lithium rechargeable battery was assembled using $LiCoO_2$ and lithium metal as the cathode active material and anode, respectively. The all-solid-state cells showed noticeable charge–discharge and cycle performances. In the cut-off voltage range of 4.3–3.4 V, it achieved high initial discharge capacities of 130, 110 and 90 mAh g^{-1} at 0.05, 0.1 and 0.2 C, respectively. Even after one hundred charge–discharge cycles, the discharge capacities remained high at 105, 100 and 95 mAh g^{-1}, respectively.

1. Introduction

Development of a solid-state electrolyte is one of the key issues for the research and development of the future generation batteries. This is because a class of materials enables the assembly of all-solid-state cells allowing the flexible design of the devices, enhancing both the energy and power densities [1]. However, among the solid-state electrolytes including both organic and inorganic compounds, the materials having a sufficient lithium ionic conductivity as well as stabilities in the voltage range for the battery operation are limited to a few cases [1–3].

On the other hand, room temperature ionic liquid (RTIL)–Li-salt mixture is recognized as one of the candidate electrolyte materials [4–6]. This is because this class of materials has a high ionic conductivity and wide potential window, low volatility and high stability. Recently, Watanabe's group proposed a new family of electrolytes for the lithium rechargeable battery, i.e., the equimolar complex of triethylene glycol dimethyl ether (triglyme,

* Corresponding author.
E-mail address: unemoto@tagen.tohoku.ac.jp (A. Unemoto).

0378-7753/$ – see front matter © 2013 Elsevier B.V. All rights reserved.
http://dx.doi.org/10.1016/j.jpowsour.2013.01.010

G3) or tetraethylene glycol dimethyl ether (tetraglyme, G4) with Li-salts [7–12]. Based on extensive investigations of the physicochemical properties over a wide range of Li-salt compositions, they revealed whether the equimolar mixtures of glyme and Li-salt behaved as a concentrated solution or ionic liquid solvent depending on the anion species' Lewis basicity. When the lithium salts with a weak Lewis basic, anion such as lithium bis(trifluoromethanesulfonyl)amide (LiTFSA), are mixed with glyme in an equimolar concentration, the mixture forms the equimolar complex, [Li(glyme)][TFSA], and thus behaves like RTILs [11]. They assembled lithium-ion rechargeable cells consisting of $LiCoO_2$ [7], $LiFePO_4$ [12] and sulfur [9] as the cathodes, and lithium as the anode, and confirmed excellent charge–discharge and cycle performances.

Another interesting property of the RTIL is the interaction with a second media such as solid surfaces [13–28]. RTIL–Li-salt–oxide mixtures change their states depending on the mixing ratios. For instance, the addition of silica [17–19] and fumed silica nanoparticles [18,24–28] leads to a composite of gels and quasi-solids with increasing the volume ratio of the oxides. By using the quasi-solid-state electrolytes based on RTIL–solid mixtures, various electrochemical devices such as fuel cells, dye-sensitized solar cells, electric double layer capacitors, and lithium-ion rechargeable batteries have been developed to date [26–28]. Recently, we investigated the ion dynamics, the stability and the electrolyte performances of a quasi-solid-state electrolyte containing conventional RTILs, such as 1-ethyl-3-methyl imidazolium bis(trifluoromethanesulfonyl)amide (EMI-TFSA), *N*,*N*-diethyl-*N*-methyl-*N*-(2-methoxyethyl)ammonium bis(trifluoromethanesulfonyl) amide (DEME-TFSA) and *N*-methyl-*N*-propyl piperidinium bis(trifluoromethanesulfonyl)amide (PP13-TFSA). When $LiCoO_2$ and lithium are used as the cathode active material and anode, respectively, our all-solid-state lithium rechargeable batteries exhibited good charge–discharge cycle performances [28].

In this study, we fabricated the quasi-solid-state electrolyte using the RTIL-like equimolar G4/LiTFSA complexes and fumed silica nanoparticles for use as the electrolyte of the all-solid-state lithium rechargeable cell. The performance of the quasi-solid-state composite was examined in terms of its ionic conductivity and self-diffusion coefficients. The lithium symmetric cells were assembled to investigate the stabilities of the quasi-solid-state electrolyte to lithium electrodes. The all-solid-state lithium-ion battery was assembled using $LiCoO_2$ and lithium metal as the cathode and anode, respectively. The charge–discharge characteristics and the cycle performances were also evaluated.

2. Experimental

2.1. Preparation of specimen

LiTFSA powder (>99%, Kishida Chemical Co., Ltd.) was dissolved into G4 (99%, Sigma–Aldrich Co.) at the desired molar ratios. These were used without further purification, but opened in an argon-filled glove box. The molar ratios of G4 to LiTFSA were 1, 2 and 8. The resultant liquids were further mixed together with fumed silica nanoparticles (390 $m^2\ g^{-1}$ specific surface area and 7 nm diameter, Sigma–Aldrich Co.) in methanol for at least 3 h. The quasi-solid-state white powder was then obtained by evaporating the methanol on a hot plate at which the temperature was kept at 323 K until the methanol was completely evaporated. Before mixing in methanol, the powder of fumed silica was dried in an oven at the temperature of 333 K for more than several days and then it was quickly transferred to and stored in the argon-filled glove box. A self-standing electrolyte sheet was obtained by further mixing the powder of polytetrafluoroethylene (PTFE, Teflon6-J, Du Pont-Mitsui Fluorochemicals Co., Ltd.) with the quasi-solid-state powder at 5 wt %. The PTFE powder was used as-received, but stored in the argon-filled glove box. The powders of the quasi-solid-state electrolyte and PTFE were weighed in the desired weight ratios and mixed using an agate mortar and an agate pestle for a few minutes until the mixtures were the self-standing transparent sheets. We also prepared the electrolyte sheets soaked in the individual G4/LiTFSA liquids. The compositions of the resultant quasi-solid-state composite powder, the self-standing electrolyte sheet and soaked in the G4/LiTFSA liquids were denoted as 75 vol% G4/LiTFSA–fumed silica (or composite), 95 wt% (75 vol% G4/LiTFSA–fumed silica)–PTFE (or composite–PTFE) and 95 wt% (75 vol% G4/LiTFSA–fumed silica)–PTFE soaked in the G4/LiTFSA liquids (or composite–PTFE (soaked)), respectively.

2.2. Evaluation of viscosity

The viscosity of the G4 and G4/LiTFSA mixtures were evaluated using a viscometer (DV-II+ Pro, Brookfield Engineering, Inc.) with a corn spindle (CPE-40) at 308 K.

2.3. Evaluation of conductivity

The electrical conductivities of the G4/LiTFSA and the apparent conductivities of the uniaxially pressed body of 75 vol% G4/LiTFSA–fumed silica with a 400 μm thickness and 10 mm diameter, 95 wt% (75 vol% G4/LiTFSA–fumed silica)–PTFE with a 200 μm thickness and 10 mm diameter, 95 wt% (75 vol% G4/LiTFSA–fumed silica)–PTFE soaked in the G4/LiTFSA liquids with a 200 μm thickness and 10 mm diameter and seven sheets of separators (#3501, Celgard LLC, denoted by separators) of 200 μm thickness and 16 mm diameter were evaluated by the two-probe ac technique. Fig. 1 shows schematic illustrations of the experimental setup and configuration for the electrical conductivity measurements of (a) the bulk and (b) the composite. A quartz tubular type holder, having two compartments, was used in this study. The individual compartment is sealed from ambient gas by O-rings. The inner quartz tube has a gas flow channel to the outer one near the bottom of the holder. A thermocouple with an alumina tube is attached near the specimen. Two potential and current probes, four in total, are inserted into the specimen and connected near the specimen in order to negate the resistance of the lead wire. The Al_2O_3 tube associated with the thermocouple is connected to the outer quartz tube by springs so that the specimen is always exposed by the mechanical pressure. The quartz holder is placed in a water bath to control the temperature.

The liquids of G4/LiTFSA mixture, i.e., "bulk" specimen, were poured into a quartz vessel of approximately 1.3 cm^3. The platinum plate electrodes having platinum lead wires were inserted into the sides of the vessel as shown in Fig. 1(a). It was placed in the "lower space" of a quartz tubular type holder. The composite powder was uniaxially pressed at 0.5 ton cm^{-2} to a 400 μm in thickness and 10 mm diameter, i.e., the "composite", was sandwiched between platinum plate electrodes with Al_2O_3 disc supports and an applied mechanical pressure uniformly from springs. It was then placed in the "upper space" of the quartz tubular type holder. The measurements were conducted in flowing argon at 100 $cm^3\ min^{-1}$. The "composite–PTFE" and "composite–PTFE (soaked)", having 200 μm thickness and 10 mm diameter, were placed in a 2032-type coin cell. The stainless steel case and spacer were used as electrodes. The specimens were connected to an electro-analytical system consisting of a potentiostat/galvanostat and a frequency response analyzer (VersaSTAT-400, Princeton Applied Research). The

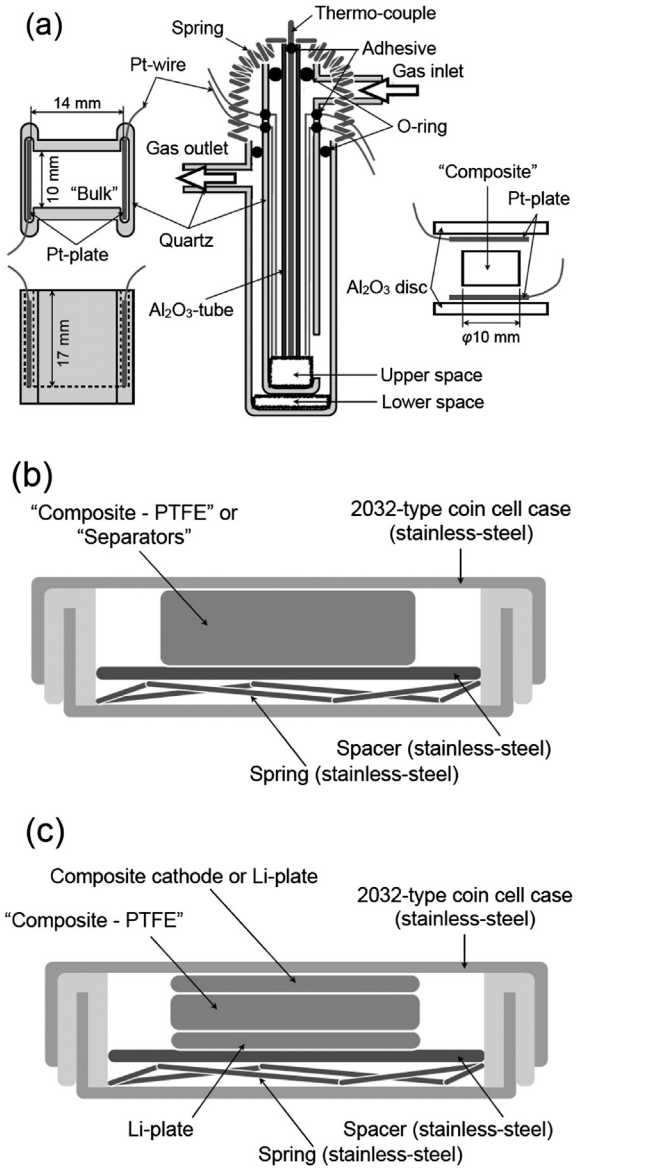

Fig. 1. Schematic illustrations of experimental setup and configuration for the electrical conductivity of (a) bulk and composite, and (b) composite–PTFE and composite–PTFE (soaked). (c) Shows the configuration of the lithium symmetric cell and battery tests.

electrolyte resistance, R, was, then, converted into the conductivity, σ, by,

$$\sigma = \frac{1}{R}\frac{L}{A} \tag{1}$$

where L and A are the distance of the electrodes and the electrode area, respectively. For the evaluation of the composites, R and σ are replaced by the apparent electrolyte resistance, $R_{app.}$, and the apparent conductivity, $\sigma_{app.}$, respectively. The temperature was first raised and kept at 353 K until stabilization of the electrical conductivity. The measurements were then conducted in the temperature range of 298–348 K with 5 K step intervals during the decreasing temperature. The applied frequency was from 1 MHz down to a spike attributed to the impedance of the blocking interfaces appears with an input voltage perturbation of 10 mV.

2.4. Evaluation of self-diffusion coefficients

The self-diffusion coefficients of the ^{1}H-, ^{19}F- and ^{7}Li-containing species in G4/LiTFSA and 75 vol% G4/LiTFSA–fumed SiO_2 were evaluated by a pulse-gradient spin-echo nuclear magnetic resonance (PGSE-NMR) technique at 298, 323 and 348 K. A Bruker Advance 400 spectrometer (Bruker BIOSPIN), equipped with a Diff60 diffusion probe (Bruker BIOSPIN), at a magnetic field of 9.4 T, was used for the measurements. The bulk specimens were poured into a 5 mm diameter glass tube. In order to avoid any convection, a small block of Teflon was placed in with the bulks. For the composites, the powders were put into a 10 mm diameter glass.

The self-diffusion coefficients were determined by Hahn's spin-echo pulse sequence using the Stejskal–Tanner relation [29],

$$\frac{S}{S_0} = \exp\left\{-\gamma^2 g^2 \delta^2 D\left(\Delta - \frac{\delta}{3}\right)\right\} \tag{2}$$

where S, δ, γ and Δ are the spin-echo signal intensity, the length of the gradient pulse, the duration of the field gradient with magnitude g, the gyromagnetic ratio, and the interval between the two gradient pulses, respectively. In this study, the repetition times, the maximum gradient values and the number of steps were fixed regardless of the compositions with 16 steps. For the evaluations of the ^{1}H-, ^{19}F- and ^{7}Li-containing species, the repetition times were 2000, 2000 and 5000 ms, respectively, and the maximum gradient values were 500, 500 and 300 G cm^{-1}, respectively. For the ^{1}H- and ^{19}F-containing species of the bulks and the composites, δ and Δ were set to 1.0–2.5 ms and 12–30 ms, respectively. For the ^{7}Li-containig species, those were set to 2.5–15 ms and 12.5–35 ms, respectively. The obtained exponential PGSE signal attenuations were then fitted by Eq. (2). The integration times for the evaluation of the ^{1}H-containing species of the bulks and the composites were 4–6 and 6–32 times, respectively. Those of the ^{19}F-containing species of the bulks and the composites were 6–8 and 12–96 times, respectively. Those of the ^{7}Li-containing species of the bulks and the composites were 8–64 and 48–1200 times, respectively. H_2O (4.877 ppm), 1 M LiCl/H_2O (0 ppm) and C_6H_5F (0 ppm) were used as the chemical shift standards of the ^{1}H, ^{7}Li and ^{19}F, respectively. The magnetic field was calibrated by the self-diffusion coefficients of the above standards at 298 K based on the literature value [30].

2.5. Evaluation of stability to lithium electrode and ion transport property

A lithium symmetric cell was assembled inside a 2032-type coin cell as schematically illustrated in Fig. 1(c). The stabilities to the lithium electrodes were evaluated by the two-probe ac and dc techniques at 308 K. A set of electro-analytical systems consisting of an Eight Channel Potentiostat/Galvanostat (1470E, Solartron Analytical)–Frequency Response Analyzer (1455A, Solartron Analytical) was used. A 95 wt% (75 vol% G4/LiTFSA)–fumed silica sheet, having a 200 μm thickness and 10 mm diameter, was sandwiched by two lithium sheet electrodes of 10 mm diameter. Before the lithium symmetric cell assembly, the electrolyte sheets were soaked in the individual G4/LiTFSA solutions. A dc potential was applied to the cells, and the ac impedance spectra were subsequently obtained at the individual dc potentials. For the ac measurements, the amplitude of the input voltage perturbation and frequencies were 10 mV and 1 M–10 mHz, respectively. For comparison, the symmetric cells with seven sheets of separators were also analyzed. For the cells with separators, the diameters of the lithium electrodes and separators were 16 mm, which is the same as that of the 2032-type coin cell inside.

2.6. Performance evaluation of all-solid-state cell

An all-solid-state cell was assembled using the 2032-type coin cell configuration as schematically illustrated in Fig. 1(c) with $LiCoO_2$ (99.8%, Sigma–Aldrich Co.) and Li (99.9%, Sigma–Aldrich Co.) as the cathode active material and anode, respectively. The powders of $LiCoO_2$ (99.8%, Sigma–Aldrich Co.), acetylene black (FX-35, Denki Kagaku Kogyo K.K.), PTFE and 75 vol% G4/LiTFSA–fumed silica were mixed using an agate mortar and an agate pestle to fabricate the composite cathode. The acetylene black powder was dried and stored in a vacuum open whose temperature was kept at 433 K. The weight ratios of the above materials were 34%, 11%, 45% and 10%, respectively. The composite cathode, the quasi-solid-state electrolyte and lithium anode was cut into 7 mm, 10 mm and 10 mm diameters respectively, and then used for assembling the all-solid-state cell. Before the all-solid-state cell assembly, the electrolyte sheet and the composite cathodes were soaked in the G4/LiTFSA solutions. The charge–discharge characteristics were evaluated by an 8CH charge/discharge unit (HOKUTO Denko Corp.) at 308 K and 0.05 C, 0.1 C and 0.2 C. 0.1 C which corresponds to an applied current density of approximately 40 μA cm^2 to the lithium anodes.

3. Results and discussion

3.1. Specimen

Fig. 2(a)–(c) shows photographs of the equimolar complex, G4/LiTFSA, the quasi-solid-state composite powder, 75 vol% G4/LiTFSA–fumed SiO_2, and the sheet, 95 wt% (75 vol% G4/LiTFSA)–fumed SiO_2–PTFE, respectively. Similar to the RTIL–Li-salt–fumed silica mixtures [26–28], our composite became a white powder even if it contains a high liquid phase concentration such as 75 vol% regardless of the molar concentrations of the G4/LiTFSA. Further introduction of a small concentration of PTFE powder, i.e. 5 wt%, leads to a self-standing transparent sheet of 200 μm thickness.

3.2. Electrical conductivities, viscosities and self-diffusion coefficients

Fig. 3 shows the typical ac impedance spectra of the SUS|composite–PTFE|SUS, SUS|composite–PTFE (soaked)|SUS and Li|composite–PTFE (soaked)|Li obtained at 308 K. For the specimens with stainless steel electrodes, the impedance consisted of a series of a resistor and a spike. The former and the latter are considered to be due to the electrolyte resistance and the impedance of the blocking interfaces. Thus, the apparent electrolyte resistance was evaluated by determining the intercept of the spike on the *x*-axis. On the other hand, when the lithium electrodes were

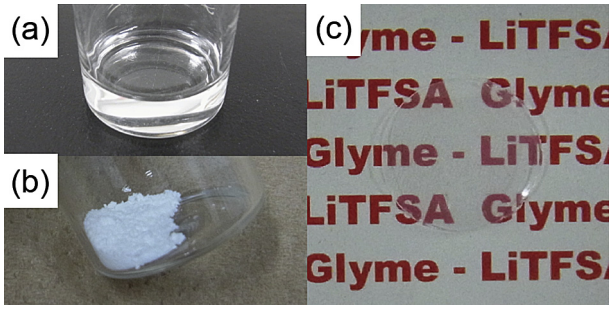

Fig. 2. Typical photographs of (a) the equimolar complex, G4/LiTFSA, (b) the composite electrolyte powder, 75 vol% G4/LiTFSA–fumed silica, and (c) the self-standing transparent electrolyte sheet, 95 wt% (75 vol% G4/LiTFSA–fumed silica)–PTFE.

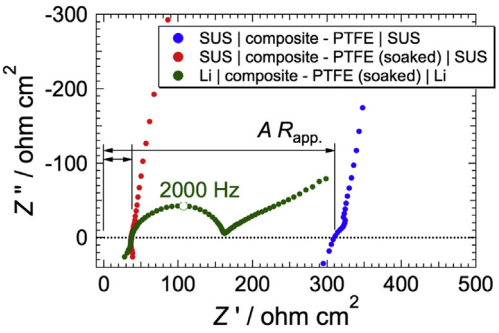

Fig. 3. Typical ac impedance spectra of SUS|composite–PTFE|SUS, SUS|composite–PTFE (soaked)|SUS and Li|composite–PTFE (soaked)|Li at 308 K.

used, a semi-circle appeared. This is considered to be due to the charge transfer resistance at the electrode/electrolyte interface. When the composite–PTFE was soaked in the G4/LiTFSA liquids, the electrolyte resistance minimized. This suggests that open pores exist in the as-synthesized composite–PTFE. By the soaking in the liquids, the open pores were filled by the liquids. As a result, the concentration of conduction phase increased, and thus it led to the minimizing the apparent electrolyte resistance.

Fig. 4 compares the electrical conductivity of the G4/LiTFSA bulks and the apparent conductivity of the uniaxially pressed body of 75 vol% G4/LiTFSA–fumed silica (composite), the sheet of 95 wt% (75 vol% G4/LiTFSA–fumed silica)–PTFE (composite–PTFE and composite–PTFE (soaked)) and seven sheets of separators (separators) as a function of the inverse temperature. Fig. 4(a)–(c) displays the conductivities of the specimens with the G4 to LiTFSA molar ratios of 1, 2 and 8, respectively. The G4/LiTFSA mixtures exhibited a VTF-type temperature dependence [31,32]. That is,

$$\sigma = A\exp\left(-\frac{B}{T-T_0}\right) \tag{3}$$

where A and B are constants related to the carrier concentrations and the apparent activation energy. T_0 is the temperature at which the ionic motion is frozen. In composite materials, loss of the conduction phase, i.e., G4/LiTFSA in this case, by the introduction of the matrix oxides or the separators need to be taken into consideration. When the volume fraction of a conduction phase exceeds the percolation threshold, the apparent conductivity is expressed by the Archie's law [33]. That is,

$$\frac{\sigma_{\text{app.}}}{\sigma} = a\varphi^m \tag{4}$$

where σ and φ are the conductivity of the conduction phase and the volume fraction of conduction phase, respectively. a has a linear relationship on a σ/σ_0 and φ in logarithmic scale. m represents the cementation index. It is reported that Eq. (4) holds for the aqueous solutions–Al_2O_3 [33] and the RTIL–silica or fumed silica [18]. The substitution of Eq. (4) into Eq. (3) leads,

$$\sigma_{\text{app.}} = a\varphi^m A\exp\left(-\frac{B}{T-T_0}\right) \tag{5}$$

The VTF-parameters, A, B and T_0, of the G4/LiTFSA mixtures, composites, composite–PTFEs, composite–PTFEs (soaked) and separators are summarized in Table 1. In this table, the constant A was replaced by $a\varphi^m A$ based on Eq. (5) except for the bulks. The volume ratio of the conduction phase was assumed to be a constant and the geometry of the conduction phase is unchanged in the investigated temperature range. The solid curves in Fig. 4 are drawn

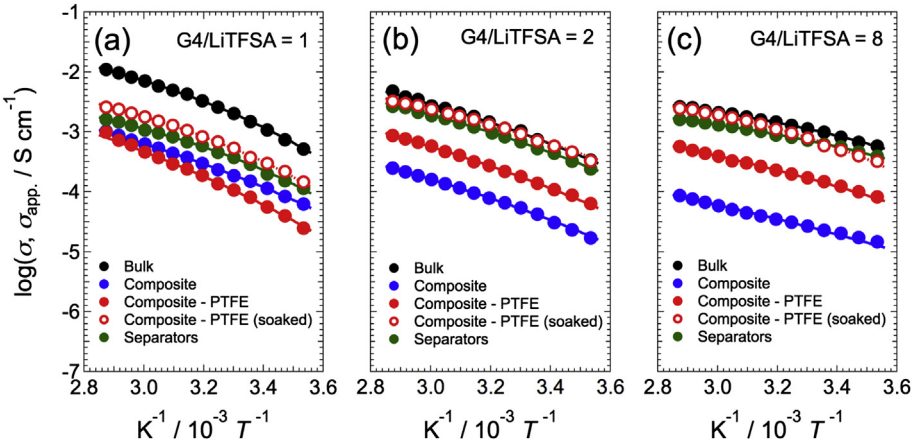

Fig. 4. The electrical and apparent conductivities of G4/LiTFSA, 75 vol% G4/LiTFSA–fumed silica, 95 wt% (75 vol% G4/LiTFSA–fumed silica)–PTFE, 95 wt% (75 vol% G4/LiTFSA–fumed silica)–PTFE soaked in the liquid and seven separators, denoted by bulk, composite, composite–PTFE, composite–PTFE (soaked) and separators, respectively, as functions of the inverse temperature. The molar ratios of G4 to LiTFSA are 1, 2 and 8 for (a), (b) and (c), respectively.

based on Eqs. (3) and (5) and the VTF-parameters summarized in Table 1.

At 308 K, the viscosity of the neat G4 was 2.65 mPa s. The viscosity monotonically increased with the decreasing G4/LiTFSA molar ratio. They were 4.94, 21.2 and 62.5 mPa s for G4/LiTFSA = 1, 2 and 8, respectively. This trend is in good agreement with the report by Yoshida et al. [10]. The specimens with different compositions had different temperature dependence of the electrical conductivities. The temperature dependence of the viscosity became significant when the molar ratio, the G4/LiTFSA increased, in other words the viscosity increased. This trend is similar to the pseudo-ternary mixtures of the TFSA-based RTIL–LiTFSA–fumed silica nanoparticles [28]. On the other hand, the order of the conductivity depended on the temperature. According to Yoshida et al., when the LiTFSA concentration is varied at a constant temperature of 303 K, the electrical conductivity of glyme–LiTFSA has maximum at a concentration of approximately 1 mol dm^{-3}. The conductivity increase up to the LiTFSA concentration of 1 mol dm^{-3} is due to the increase in the carrier species. The conductivity decrease by a further increase in the LiTFSA concentration is then due to the decreased mobility of the ionic species by the increased viscosity [10]. Thus, the variation in the order of the conductivity depending on temperature, seen in Fig. 4, might be due to the temperature dependences of both the carrier concentrations and the viscosities.

The apparent conductivities of the uniaxially pressed body of the 75 vol% G4/LiTFSA–fumed silica (composite), the sheet of 95 wt % (75 vol% G4/LiTFSA–fumed silica)–PTFE (composite–PTFE and composite–PTFE (soaked)) and seven sheets of separators (separators) were lower than those of the bulk. As summarized in Table 1, the B and T_0 values of the separators and the composite–PTFE (soaked) were similar to those of the bulks regardless of the compositions. This means that the decreases in the apparent conductivity of the separators are mainly due to the volume loss of the conduction phase. On the other hand, B and T_0 of the composite and the composite–PTFE tended to be higher and lower, respectively, than those of the bulks. These deviations were greater than the structural differences from the bulks and the separators. Thus, it is expected that the ion transport properties in the composite and the composite–PTFE are essentially different from the bulks.

In order to examine the effect of the fumed silica addition to the G4/LiTFSA mixtures on the ion dynamics, the self-diffusion coefficients were evaluated. Fig. 5(a)–(c) is the self-diffusion coefficients of the constituent species, i.e., the ^{1}H-, ^{19}F- and ^{7}Li-containing species of the G4/LiTFSA mixtures and the quasi-solid-state 75 vol% G4/LiTFSA–fumed silica composites at 298, 323 and 348 K, respectively. For the G4/LiTFSA mixtures, the self-diffusion coefficients monotonically increased with the increasing G4/LiTFSA molar ratios due to the enhanced mobility of the diffusing species by the decreasing viscosity.

According to Tamura et al., the self-diffusion coefficients of the ^{1}H-, ^{19}F- and ^{7}Li-containing species of the equimolar complex of G4 and LiTFSA are log (D_H/m^2 s^{-1}) = −10.90, log (D_F/m^2 s^{-1}) = −10.90 and log (D_{Li}/m^2 s^{-1}) = −10.91, respectively, at 308 K [8]. They concluded that Li^+ and $TFSA^-$ are coordinated with one G4 solvent molecule, and thus forms the [Li(G4)][TFSA] complex [7–12]. In our measurements at 298 K, the self-diffusion coefficients of our G4/LiTFSA bulk were log (D_H/m^2 s^{-1}) = −10.46, log (D_F/m^2 s^{-1}) = −10.48 and log (D_{Li}/m^2 s^{-1}) = −10.56, similar to the report by Tamura et al. in terms of both the absolute values and the insignificant differences among the ^{1}H-, ^{19}F- and ^{7}Li-containing species. With the increasing molar ratio of G4/LiTFSA, the differences in the self-diffusion coefficients of the constituent species tended to be higher and the order of the self-diffusion coefficients

Table 1
Summary of the VTF-parameters and the maximum current density for lithium electrode with the G4/LiTFSA at 308 K.

Composition	A or $a\varphi^m$ A/S cm^{-1}	B/K^{-1}	T_0/K	$j_{max.}$/μA cm^{-2}
G4/LiTFSA = 1				
Bulk	6.0×10^{-1}	6.0×10^{2}	2.0×10^{2}	–
Composite	2.0×10^{-1}	1.0×10^{3}	1.6×10^{2}	–
Composite–PTFE	4.8×10^{-1}	1.2×10^{3}	1.6×10^{2}	–
Composite–PTFE (soaked)	1.1×10^{-1}	5.5×10^{2}	2.0×10^{2}	146
Separators	4.6×10^{-2}	4.8×10^{2}	2.0×10^{2}	115
G4/LiTFSA = 2				
Bulk	4.5×10^{-1}	8.5×10^{2}	1.7×10^{2}	–
Composite	3.8×10^{-2}	9.6×10^{2}	1.6×10^{2}	–
Composite–PTFE	1.8×10^{-1}	1.0×10^{3}	1.5×10^{2}	–
Composite–PTFE (soaked)	1.8×10^{-1}	7.2×10^{-1}	1.7×10^{-1}	64
Separators	2.1×10^{-1}	7.8×10^{2}	1.7×10^{2}	37
G4/LiTFSA = 8				
Bulk	1.9×10^{-2}	2.9×10^{2}	2.0×10^{2}	–
Composite	9.7×10^{-3}	1.1×10^{3}	1.2×10^{2}	–
Composite–PTFE	3.2×10^{-2}	8.1×10^{2}	1.5×10^{2}	–
Composite–PTFE (soaked)	2.5×10^{-2}	3.1×10^{2}	2.1×10^{2}	31
Separators	1.2×10^{-2}	3.1×10^{2}	1.9×10^{2}	16

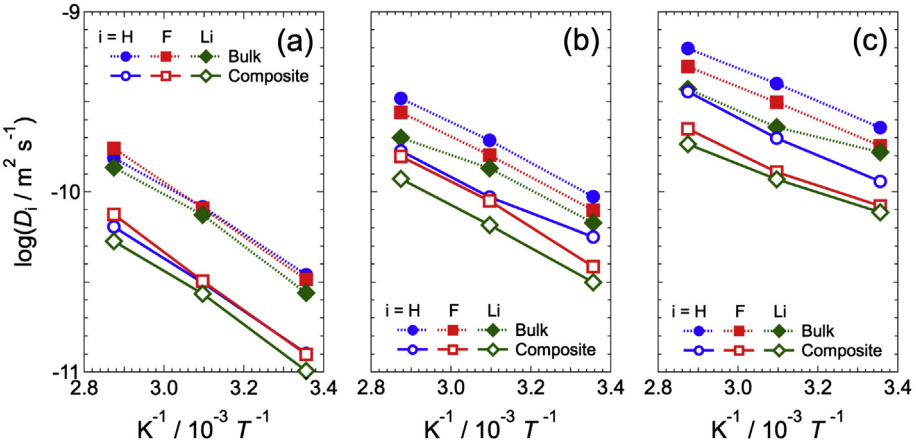

Fig. 5. The self-diffusion coefficients of species i (=^{1}H, ^{19}F and ^{7}Li) in G4/LiTFSA and 75 vol% G4/LiTFSA–fumed silica as functions of the inverse temperature. The molar ratios of G4 to LiTFSA are 1, 2 and 8 for (a), (b) and (c), respectively.

was the H-, F- and Li-containing species. This order is similar to the conventional liquid electrolyte containing organic liquid–Li-salt mixtures with comparatively larger viscosity and dielectric constants, which enhances the dissociation degrees of the lithium salts [34]. This trend also continued for the quasi-solid-state electrolyte composition. The self-diffusion coefficients of the 75 vol% G4/LiTFSA–fumed silica were log (D_H/m^2 s^{-1}) = −10.90, log (D_F/m^2 s^{-1}) = −10.90 and log (D_{Li}/m^2 s^{-1}) = −10.99 with the equimolar composition at 298 K, and then the difference in the self-diffusion coefficients of the constituent species became higher with the increasing G4/LiTFSA ratios. Differences in the self-diffusion coefficients between the bulk and the quasi-solid-state composite are insignificant compared to the composition dependence of the self-diffusion coefficients. These results suggest that the equimolar mixture essentially forms an equimolar complex similar to the bulk in the quasi-solid-state electrolyte while the fumed silica surface slows the ion dynamics.

Taking all these results into consideration, the decrease in the apparent conductivity of the composites compared to bulk is caused by not only the decrease in the ion transport phase, but also the slow effect of the ion transport at the fumed silica surfaces.

3.3. Anodic stability under polarization and resistance analysis

In this study, we used ac and dc techniques to evaluate the anodic stability by the lithium symmetric cells. This is because the determination of the anodic stability in our cell configuration by the classical voltammetric technique has the following problems: (1) The voltage drop mainly occurs in the quasi-solid-state electrolyte during current flow as discussed below. Thus, there needs to place the reference electrode just beneath the working electrode. However, this is quite difficult to do because the quasi-solid-state film electrolyte, having a 200 μm thickness, is used. (2) The concentration profile inside the electrolyte depends on the electrolyte structure. Actually, the contribution of the concentration polarization resistance depends on the electrolyte structures as discussed below. Therefore, even if the lithium counter electrode having higher surface areas versus the working electrode is applied with a two-probe cell configuration, the concentration profile inside the electrolyte in such cells may be different from that inside the all-solid-state cells. In addition, the significant contribution of the voltage drop inside the quasi-solid-state electrolyte obscures the meaning of the voltage axis. (3) The measurement requires the working electrode to be inactive to lithium, such as gold, stainless steel, nickel etc., although reductive decomposition occurs at the lithium/electrolyte interface. It was reported by Zheng et al. that the potential window depends on the electrode materials [35,36]. In addition, in such measurements, it is difficult to separately evaluate the contributions of the reductive decomposition and ionic currents only by the coulombic efficiency of the lithium deposition and dissolution. Thus, utilization of lithium as the working electrode is preferential in order to determine the reductive stability under actual working conditions of the all-solid-state cells.

On the other hand, the dc measurements determines us the degree of the reductive decomposition at the lithium/electrolyte interface in the current profile at a constant voltage. Fig. 6 shows the typical current of the lithium symmetric cells with the quasi-solid-state electrolyte, 95 wt% (75 vol% G4/LiTFSA–fumed silica)–PTFE (soaked), at 308 K under the applied voltages of 150 and 200 mV. The features of the current profile depend on the applied voltages. The current reached a steady-state at the applied voltages below 150 mV within 1 h, while it did not under the applied voltage of 200 mV. The latter profile contained scatterings and gradual increases in the current density. The unusual current profiles suggest that the quasi-solid-state electrolyte is unstable to the lithium electrode at the applied voltage and the contribution of the reductive decomposition current is significant at that applied voltage. This means that, in order to inhibit the contribution of the anodic decomposition during battery operation, the applied current needs to be below 146 μA cm^{-2} for the lithium anode. We

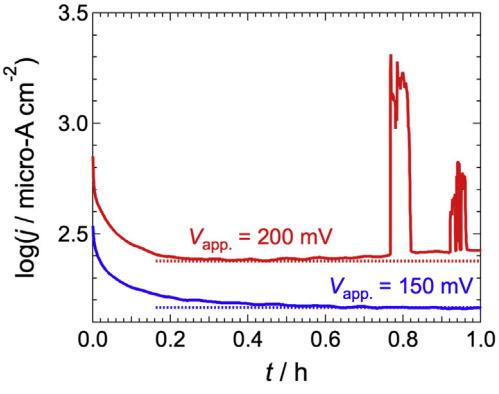

Fig. 6. Typical current profiles of the lithium symmetric cell using 95 wt% (75 vol% G4/LiTFSA–fumed silica)–PTFE (soaked) at the applied voltages of 150 mV and 200 mV as a function of time at 308 K.

define here this value as the maximum current density, $j_{max.}$; at which the contribution of the reductive decomposition current is negligible.

Investigation of the stability using the symmetric cell also has a problem because it is not known how much a voltage drop occurs at the individual electrode/electrolyte interfaces. However, this might be sufficient because a typical battery test is conducted by applying a constant current. Based on this idea, we evaluated the reductive stability of the quasi-solid-state electrolyte consisting of 95 wt% (75 vol% 1 M LiTFSA–EMI-TFSA–fumed silica)–PTFE. It was found that when the applied current exceeds $j_{max.}$ during the battery tests, the coulombic efficiency of the all-solid-state cells obviously decreased. The decrease was more remarkable by increasing the applied current [28]. Table 1 summarizes the maximum current density of the quasi-solid-state electrolytes as a function of the G4/LiTFSA molar ratio. In this table, the values of the lithium symmetric cells with the seven sheets of separators are also summarized. The maximum current increased with the decreasing G4/LiTFSA molar ratio. The values of the composite and the separators with the equimolar complex exhibited the highest values at the different G4/LiTFSA molar ratios. These results suggest that not only the cathodic stability [7–9,11], but also the anodic stability are enhanced by the equimolar compositions. The anodic stability of the quasi-solid-state composite electrolyte is superior to that of the separators. This suggests that the structure of the electrolyte is also one of the important factors determining the stability to lithium electrodes.

We also evaluated the maximum current densities of the lithium electrodes in the RTIL-based quasi-solid-state composites, 95 wt% (75 vol% 1 M LiTFSA/cation-TFSA–fumed silica)–PTFE, at 308 K, where cation = EMI, DEME and PP13 [28]. They were 24, 126 and 55 μA cm^2, respectively. Among the quasi-solid-state electrolytes we investigated, the quasi-solid-state composite containing the equimolar complex of G4/LiTFSA exhibited the highest values.

As seen in Fig. 3, the impedance spectra of the lithium symmetric cells with the equimolar G4/LiTFSA containing quasi-solid-state electrolyte had an ohmic resistance, a semi-circle and a spike, corresponding to the electrolyte, the charge transfer and the concentration polarization resistances, respectively. The features of the impedance spectra were similar to the report by Yoshida et al. [10]. For instance, when the applied voltage is 10 mV at 308 K, the ohmic and charge transfer resistances were 20.6 and 217 Ω cm^2, respectively, while the total resistance, evaluated by the steady-state resistance and the applied voltage was 865 Ω cm^2. This suggests that the concentration polarization resistance is remarkable under polarization, similar to the quasi-solid-state composites containing 1 M LiTFSA/cation-TFSA (cation = EMI, DEME and PP13) [28]. The contribution of the concentration polarization was evaluated by the equation, $R_{pol.}/R_{ct.} + R_{pol.}$, where $R_{ct.}$ and $R_{pol.}$ are the resistances of the charge transfer and the concentration polarization, respectively. The total resistance, R_t, was evaluated by the steady-state current, $j_{st.}$, at the applied voltage, $V_{app.}$, i.e., $R_t = V_{app.}/j_{st.}$. The electrolyte resistance, $R_{el.}$, and the charge transfer resistance, $R_{ct.}$, are then subtracted from R_t to derive the concentration polarization resistance, $R_{pol.}$. The values are in the ranges of 0.65–0.76 for the quasi-solid-state electrolyte, which is comparable to or smaller than the quasi-solid-state composites containing 1 M LiTFSA/cation-TFSA for 0.70–0.76, 0.87–0.91 and 0.87–0.91 for cation = EMI, DEME and PP13, respectively [28]. When the highly viscous liquids are used, the contribution of the concentration polarization tended to be significant. This suggests that the slow transport of lithium ions in the quasi-solid-state electrolyte limits the devices' power density similar to the RTIL–Li-salt systems [6].

3.4. Battery performances

Fig. 7 shows the initial charge–discharge profiles of the all-solid-state cells containing the quasi-solid-state electrolytes having the equimolar G4/LiTFSA at 0.05 C and 308 K. For a comparison, the profile of the cell with a conventional organic liquid electrolyte, i.e., 1 M $LiClO_4$ in EC:DEC (1:1 in volume), with a separator at the charge rate of 0.5 C is shown in the figure. As expected by the all-solid-state battery using the RTIL-based quasi-solid-state electrolytes [26–28], the all-solid-state cells consisting of the quasi-solid-state electrolytes with 95 wt% (75 vol% G4/LiTFSA–fumed silica)–PTFE (soaked) have successfully worked as a rechargeable battery, while the discharge capacity was only 90 mAh g^{-1} in the investigated voltage range. It is clear from the figure that the all-solid-state cell containing the equimolar G4/LiTFSA had a higher potential drop than the cell containing an organic liquid electrolyte, resulting in an insufficient compositional change in the cathode active material. The main cause of the larger potential drop might be the slower lithium-ion transport as already evaluated. Therefore, we also examined the performance at the increasing cut-off voltage of 4.3 V. As a result, the discharge capacity increased from 90 to 130 mAh g^{-1}, which is similar to the cells with the EMI-TFSA-based quasi-solid-state electrolytes of 110–130 mAh g^{-1} [28], the equimolar complex of G4/LiTFSA [7] and the organic electrolyte with a separator of 140 mAh g^{-1} at 0.5 C. Therefore, the evaluation of the charge–discharge characteristics of G4/LiTFSA was conducted in the cut-off voltage range of 3.4–4.3 V.

The 1st–100th charge–discharge profiles of the all-solid-state cells with 95 wt% (75 vol% G4/LiTFSA–fumed silica)–PTFE (soaked) at 308 K and 0.05 C, 0.1 C and 0.2 C are shown in Fig. 8(a)–(c), respectively. The initial discharge capacities at 0.1 and 0.2 C were 110 and 90 mAh g^{-1}, respectively. The values were comparable to the typical RTIL-based quasi-solid-state electrolytes [26,28] and the equimolar complex of G4/LiTFSA with a separator [7]. The all-solid-state cells achieved a stable battery operation for the one hundred charge–discharge cycles at every *c*-rate. At the 100th cycle, the discharge capacities at 0.05, 0.1 and 0.2 C were 105, 100 and 95 mAh g^{-1}, respectively. The discharge capacity retentions of the 10th, 30th, 50th and 100th cycles were 95%, 89%, 87% and 80%, respectively, for 0.05 C, and were 97%, 93%, 95% and 94%, respectively, for 0.1 C. At 0.2 C, the discharge capacity gradually increased with the increasing cycle numbers up to 9 cycles, then reached 105 mAh g^{-1}. The discharge capacity retentions of 30th, 50th and 100th cycles to the 9th cycle were 93%, 90% and 89%, respectively. The decreases in the discharge capacity retentions

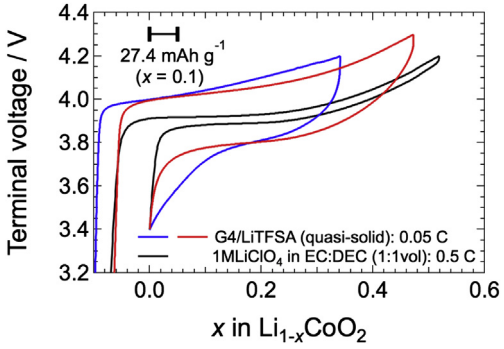

Fig. 7. The initial charge–discharge profiles of the all-solid-state cells using 95 wt% (75 vol% G4/LiTFSA–fumed silica)–PTFE (soaked) as electrolytes at 0.05 C and 308 K as a function of *x* in $Li_{1-x}CoO_2$. The profiles of the cell with a conventional liquid electrolyte with a separator obtained at 0.5 C are also shown for comparison.

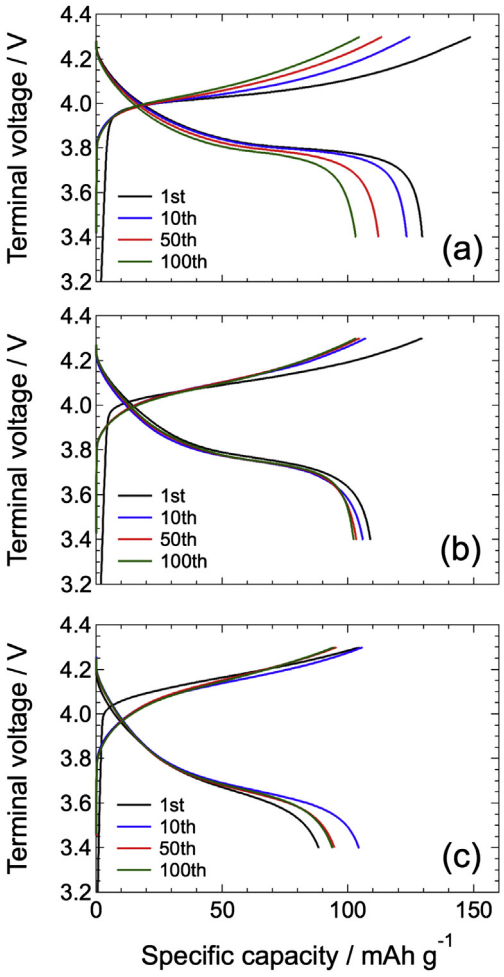

Fig. 8. The 1st–100th charge–discharge profiles of the all-solid-state cells using 95 wt % (75 vol% G4/LiTFSA–fumed silica)–PTFE (soaked) as electrolytes at (a) 0.05 C, (b) 0.1 C and (c) 0.2 C at 308 K.

with a few tens of charge–discharge cycles are more remarkable than those after the 30th cycle for all the *c*-rates.

The coulombic efficiencies of the initial cycles were low at 87%, 84% and 85% for 0.05, 0.1 and 0.2 C, respectively. They then increased after a few tens of charge–discharge cycles to be above 98% at every *c*-rate. This trend is similar to the lithium rechargeable cells using the RTIL–Li-salt mixtures as electrolytes [4,5]. The average coulombic efficiency from the 50–100 cycles increased with the increasing *c*-rates. The average values were 98.6, 99.1 and 99.5% for 0.05, 0.1 and 0.2 C, respectively. As seen in Fig. 6, the all-solid-state cells with 0.05 C exhibited the highest decrease in the discharge capacity retention and poor coulombic efficiency. As evaluated in the previous chapter, the current density, whose contribution by the reductive decomposition at the lithium anode, is far greater than those applied for battery operation. Thus, it might be considered that the higher decrease in the discharge capacity retention and poor coulombic efficiency might be due to the contribution of the oxidative decomposition of the quasi-solid-state electrolytes because the electrode/electrolyte interface is exposed to a higher voltage due to lower voltage drop for a longer period by application of the lower *c*-rates.

As discussed above, the lithium-ion cells with a conventional organic electrolyte exhibited a superior power density compared to our all-solid-state cells containing G4/LiTFSA, similar to those containing 1 M LiTFSA/cation-TFSA (cation = EMI, DEME and PP13) [28] as well as the lithium cells using the RTIL–Li-salt mixture with a separator [4–6]. Thus, in order to achieve a higher power density, enhancement of the lithium-ion transport in the quasi-solid-state electrolyte is required in future studies.

4. Conclusions

In this study, the quasi-solid-state composites consisting of 75 vol% G4/LiTFSA–fumed silica nanoparticles were prepared for use as electrolytes in an all-solid-state lithium rechargeable battery. The quasi-solid-state electrolytes have liquid-like high ionic conductivities and self-diffusivities, while the solid surfaces somewhat slowed the ion transport. Compared to the quasi-solid-state electrolyte containing the conventional RTIL–LiTFSA mixtures, that containing the equimolar G4/LiTFSA exhibited the highest stability to the lithium electrode during polarization. Our all-solid-state cells with the quasi-solid-state electrolytes have achieved a high discharge capacity and stable cycle performances. However, compared to the conventional organic electrolyte, the power density was insufficient, similar to the cells with the RTIL-based electrolytes due to remarkable contribution of the concentration polarization. In order to enhance the power density, the mitigation of the concentration polarization is highly requested in future studies.

Acknowledgements

This study was supported by the MIKIYA Science and Technology Foundation, the Funding Program for World-Leading Innovative R&D on Science and Technology (FIRST), “Innovative Basic Research Toward Creation of High-Performance Battery”, and a Grant-in-Aid for Young Scientist (B) from the Japan Society for the Promotion of Science.

References

[1] Y. Kato, K. Kawamoto, R. Kanno, M. Hirayama, Electrochemistry 80 (2012) 749.
[2] J.W. Fergus, J. Power Sources 195 (2010) 4554–4569.
[3] N. Kamaya, K. Homma, Y. Yamakawa, M. Hirayama, R. Kanno, M. Yonemura, T. Kamiyama, Y. Kato, S. Hama, K. Kawamoto, A. Mitsui, Nat. Mat. 10 (2011) 682–686.
[4] H. Sakaebe, H. Matsumoto, Electrochem. Commun. 5 (2003) 594–598.
[5] H. Sakaebe, H. Matsumoto, K. Tatsumi, J. Power Sources 146 (2005) 693–697.
[6] H. Matsumoto, H. Sakaebe, K. Tatsumi, M. Kikuta, E. Ishiko, M. Kono, J. Power Sources 160 (2006) 1308–1313.
[7] K. Yoshida, M. Nakamura, Y. Kazue, N. Tachikawa, S. Tsuzuki, S. Seki, K. Dokko, M. Watanabe, J. Am. Chem. Soc. 133 (2011) 13121–13129.
[8] T. Tamura, K. Yoshida, T. Hachida, M. Tsuchiya, M. Nakamura, Y. Kazue, N. Tachikawa, K. Dokko, M. Watanabe, Chem. Lett. 39 (2010) 753–755.
[9] N. Tachikawa, K. Yamauchi, E. Takashima, J.-W. Part, K. Dokko, M. Watanabe, Chem. Commun. 47 (2011) 8157–8159.
[10] K. Yoshida, M. Tsuchiya, N. Tachikawa, K. Dokko, M. Watanabe, J. Phys. Chem. C 115 (2011) 18384–18394.
[11] K. Ueno, K. Yoshida, M. Tsuchiya, N. Tachikawa, K. Dokko, M. Watanabe, J. Phys. Chem. B 116 (2012) 11323–11331.
[12] S. Seki, K. Takei, H. Miyashiro, M. Watanabe, J. Electrochem. Soc. 158 (2011) A769–A774.
[13] T. Fukushima, A. Kosaka, Y. Ishimura, T. Yamamoto, T. Takigawa, N. Ishii, T. Aida, Science 300 (2003) 2072–2074.
[14] T. Katakabe, T. Kaneko, M. Watakane, T. Fukushima, T. Aida, J. Electrochem. Soc. 152 (2005) A1913–A1916.
[15] M.-A. Neouze, J. LeBideau, A. Vioux, Prog. Solid State Chem. 33 (2005) 217–222.
[16] M.-A. Neouze, J. LeBideau, P. Gaveau, S. Bellayer, A. Vioux, Chem. Mater. 18 (2006) 3831–3936.
[17] T. Katakabe, R. Kawano, M. Watanabe, Electrochem. Solid-State 10 (2007) F23–F25.
[18] S. Shimano, H. Zhou, I. Honma, Chem. Mater. 19 (2007) 5216–5221.
[19] Y. Saito, T. Umecky, J. Niwa, T. Sakai, S. Maeda, J. Phys. Chem. B 111 (2007) 11794–11802.
[20] U.-H. Lee, T. Kudo, I. Honma, Chem. Commun. (2009) 3068–3070.
[21] T. Echelmeyer, H.W. Meyer, L. van Wullen, Chem. Mater. 21 (2009) 2280–2285.
[22] M. Mezger, H. Schroder, H. Reichert, S. Schramm, J.S. Okasinski, S. Schoder, V. Honkimaki, M. Deutsch, B.M. Ocko, J. Ralstron, M. Rohwerder, M. Stratmann, H. Dosch, Science 322 (2008) 424–428.
[23] K. Ueno, M. Kasuya, M. Watanabe, M. Mizukami, K. Kurihara, Phys. Chem. Chem. Phys. 12 (2010) 4066–4071.

[24] A. Unemoto, Y. Iwai, S. Mitani, S.-W. Baek, S. Ito, T. Tomai, J. Kawamura, I. Honma, Solid State Ionics 201 (2011) 11–20.
[25] A. Unemoto, Y. Iwai, S. Mitani, S.-W. Baek, S. Ito, T. Tomai, J. Kawamura, I. Honma, Solid State Ionics 225 (2012) 416–419.
[26] S. Ito, A. Unemoto, H. Ogawa, T. Tomai, I. Honma, J. Power Sources 208 (2012) 271–275.
[27] H. Ogawa, A. Unemoto, I. Honma, Electrochemistry 80 (2012) 765–767.
[28] A. Unemoto, H. Ogawa, S. Ito, I. Honma, J. Electrochem. Soc. 160 (2013) A138–A147.
[29] E.O. Stejskal, J.E. Tanner, J. Chem. Phys. 42 (1965) 288–292.
[30] M. Holz, H. Weingartner, J. Magn. Reson. 92 (1969) 115–125.
[31] H. Vogel, Phys. Z. 22 (1921) 645.
[32] G.S. Fulcher, J. Am. Ceram. Soc. 8 (1925) 339–355.
[33] S. Deki, M. Mizuhata, K. Nakamura, A. Kajinami, Y. Kanaji, J. Electrochem. Soc. 139 (1992). 1554–1548.
[34] K. Hayamizu, Y. Aihara, S. Arai, C.G. Martinez, J. Phys. Chem. B 103 (1999) 519–524.
[35] H. Zheng, H. Zhang, Y. Fu, T. Abe, Z. Ogumi, J. Phys. Chem. B 109 (2005) 13676–13684.
[36] H. Zheng, J. Qin, Y. Zhao, T. Abe, Z. Ogumi, Solid State Ionics 176 (2005) 2219–2226.